Composites Part B 278 (2024) 111425

Contents lists available at ScienceDirect

Composites Part B

journal homepage: www.elsevier.com/locate/compositesb

Superior photoluminescence of quantum dot displays via organic-inorganic composite scatterers

MinSu Kim [a,1,*], DaYeon Lee [a,1], HaYoung Jung [a], Seung Hee Lee [a,b,c,**]

[a] Department of Nano Convergence Engineering, Jeonbuk National University, Jeonju, Jeonbuk, 54896, Republic of Korea
[b] Department of Polymer-Nano Science and Technology, Jeonbuk National University, Jeonju, Jeonbuk, 54896, Republic of Korea
[c] Department of JBNU-KIST Industry-Academia Convergence Research, Jeonbuk National University, Jeonju, Jeonbuk, 54896, Republic of Korea

ARTICLE INFO

Handling Editor: Prof. Joong Lee

Keywords:
Quantum dots
Quantum dot organic light-emitting diodes (QD-OLEDs)
External quantum efficiency
Color conversion efficiency
Liquid crystals

ABSTRACT

High color purity of quantum dot organic light-emitting diodes (QD-OLEDs) can be achieved by blue OLED light to stimulate pixelized green and red QDs within a color conversion layer, providing high color conversion efficiency in commercialized displays. However, enhancing external quantum efficiency (EQE) and minimizing blue light leakage remain significant challenges. To resolve these issues, we have developed an organic-inorganic composite system comprising quantum dots (QDs), liquid crystal (LC), polymer, and inorganic nanoparticles, like titanium dioxide (TiO_2). The best EQE was enhanced by ~81.9% when TiO_2 of 6 wt%. More importantly, the EQE was enhanced by ~58.6% when TiO_2 of 3 wt% while TiO_2 nanoparticles were well-dispersed and stable without aggregation for more than 3 days, which is crucial for preventing nozzle blockages during inkjet printing in manufacturing processes. We believe our innovative approach is promising for boosting color conversion efficiency by exciting highly concentrated green and red QDs with blue light while also overcoming inherent fabrication hurdles associated with high concentrations of inorganic scatterers.

1. Introduction

The pursuit of authentic color representation through display devices is an ongoing endeavor. Non-emissive liquid crystal displays (LCDs) [1], which use color filters to display colors, can enhance color purity by incorporating a red and green colloidal quantum dot (QD)-embedded polymer film on a backlight unit. For instance, QD enhancement films (QDEFs), composed of red and green QDs dispersed in a polymer matrix, have been inserted between an LC panel and a blue LED backlight to expand the color gamut of LCDs [2,3]. Emissive organic light-emitting diodes (OLEDs) demonstrate superior color gamut compared to LCDs without QDEFs due to their light-emitting organic materials' narrow full width at half maximum (FWHM) of approximately 50 nm. Colloidal QDs—nano-sized crystalline semiconductors within the exciton Bohr radius range that exhibit quantum confinement effects—are among the most promising materials for achieving high-color-purity displays due to their exceptional characteristics such as narrow FWHM (<50 nm), high quantum yield (>80%), thermal and photostability, and compatibility with solution processes like inkjet printing [4,5]. Recently, commercialized QD-OLEDs have leveraged the photoluminescence (PL) of QDs. A combination of a blue OLED with pixelized green and red QD layers has emerged as an effective method for enhancing color gamut—converting blue OLED light into green or red light within each pixel while allowing unconverted blue light to pass through non-QD pixels for blue pixels. However, even though the blue light passes through the color conversion layer, some portion penetrates without undergoing Stokes shift. This unconverted blue *leakage* interferes with achieving high-color-gamut in green and red pixels. To improve the light conversion efficiency, the blue light leakage ratio must be controlled, which can be determined as,

$$\text{Blue leakage} = \frac{I_B}{I_0} \times 100\ (\%), \tag{1}$$

where I_0 and I_B denote the measured intensity of blue light before and after passing through the QD layer, respectively. If the ratio does not reach 0%, the unconverted blue light causes color-mixing issue, correlated with emitting green and red light. In this case, color filters must be

* Corresponding author.
** Corresponding author. Department of Polymer-Nano Science and Technology, Jeonbuk National University, Jeonju, Jeonbuk 54896, Republic of Korea
E-mail addresses: minsu.kim@jbnu.ac.kr (M. Kim), lsh1@jbnu.ac.kr (S.H. Lee).
[1] These authors contributed equally to this work.

https://doi.org/10.1016/j.compositesb.2024.111425
Received 9 January 2024; Received in revised form 20 March 2024; Accepted 28 March 2024
Available online 30 March 2024
1359-8368/© 2024 Elsevier Ltd. All rights reserved.

placed above the QD layers to eliminate the blue light and to complete the color conversion leakage in commercialized QD-OLEDs. However, the color filters cause extra fabrication processes and cost. For analysis on the color-mixing issue and low efficiency of the color conversion, defining external quantum efficiency (EQE) helps quantify the phenomena based on the formula,

$$\eta_e = \frac{I_{PL}}{I_0} \times 100\ (\%), \tag{2}$$

where I_{PL} denotes photoluminescence (PL) intensity after experiencing QD layers. To enhance EQE as well as to decrease blue leakage, the incident blue light needs to be fully absorbed by QD layer and the absorbed light should be efficiently converted to emitting light. The absorbance of the layer is governed by Beer-Lambert's law as follows,

$$A = \varepsilon c d = \log T^{-1} \tag{3}$$

where ε, c, d, and T denote absorbance coefficient of QDs associated with internal photoluminescent quantum yield (PLQY), concentration of QDs, the layer thickness, and transmittance, respectively. Increasing PLQY directly influences high absorbance, which can be done by developing the QDs from a material perspective. Increasing concentration or layer thickness must be good approaches for enhancing absorbance; however, certain limitations may exist due to concentration quenching effects [6] or practical restrictions to increase the layer thickness, respectively.

Previous studies to elaborate this issue proposed surface modifications or scatterer addition techniques [7–13]. In case of surface modification, however, this method often requires specialized treatments for large-area uniformity. A more practical strategy involves forming scatterers inside the QD color conversion layers—increasing optical path length within this layer in three dimensions enhances absorption probability by unconverted incident lights for high EQE and low blue leakage ratio. To implement the idea, some approaches have been reported such as forming a mesoporous structure in a QD film or dispersing inorganic nanoparticles having a high refractive index in a QD film [7,9,10,12–14]. One effective method involves using TiO_2 nanoparticles as scatterers; however, adding these particles can cause significant problems during inkjet processes such as nozzle clogging or increased mixture viscosity due to particle aggregation or precipitation, which is a fatal flaw. Here, in our work, we propose using liquid crystal-polymer (LC-P) composites as scatterers in QD color conversion layers via polymerization-induced phase separation (PIPS) methods. This approach is highly effective to lower added amount of TiO_2 in the mixture because the LC droplets are formed as scatterers. LCs can reduce aggregation issues, which seem to be caused by high concentration of inorganic particles, and can reduce mixture viscosity, thereby avoiding critical challenges during inkjet processes. Consequently, this system increases optical path length within the conversion layer allowing more QD particles that can be involved in Stokes shift while reducing residual unconverted blue leakage. We also examined the correlation between blue light scattering and EQE using the Rayleigh-Gans approximation. The size of the LC droplets, which can be adjusted by altering the concentration of LCs and UV irradiance conditions (intensity and exposure time), significantly influences blue light scattering properties. We found the QD-LC-P system allows us to achieve high EQE, and remarkably, even higher EQE can be achieved by the combination of these organic scatterers and small amount of TiO_2 particles, thereby avoiding aggregation, precipitation, and clogging during inkjet processes while maintaining high EQE.

2. Results and discussion

2.1. Quantum dot–liquid crystal–polymer (QD-LC-P) composites

Efficient color conversion layers can be fabricated through a solution process, which involves preparing homogeneous mixtures of LC, prepolymer, and QD-toluene solution, followed by injecting this mixture between sandwiched glass substrates. The fabrication process for QD color conversion layers is depicted in Fig. 1a. After evaporating the toluene from the mixture in a vacuum, the resultant substance is injected into empty unit cells via capillary force. To evaluate the color conversion efficiency based on optical scattering achieved by LC-polymer composites, we maintained consistency in the film thickness to exclude any effects related to the cell thickness as presented in Equation (3). The average cell gap of the samples was measured at 12 ± 0.52 μm (Fig. S1), indicating consistency in unit cell thickness. We executed PIPS via UV irradiation to form optical scatterers of LC droplets within a polymer matrix. This represents the color conversion layer in QD-OLEDs as illustrated in Fig. 1b. As blue light propagates through this color conversion layer, optical scattering occurs at the interface between LC (E7) and polymer (NOA65) due to differences in refractive index ($n_{E7} = 1.5962$ and $n_{NOA65} = 1.524$, Experimental Section) as shown in Fig. 1c.

Optimizing both backward and forward scattering is essential for increasing the optical path length, which in turn enhances color conversion efficiency and reduces blue light leakage within the color conversion layer. Generally, LC and polymer (LC-P) composites predominantly exhibit forward scattering [15–19]. Montgomery Jr. and colleagues have reported that in polymer-dispersed liquid crystal (PDLC) systems, backward scattering is dependent on the ratio of droplet size to wavelength, as explained by the Rayleigh-Gans approximation [20]. The ratio of light scattering to the backward hemisphere can be expressed as,

$$B = N_v \sigma_b d = \frac{3\pi n_p d}{2} |m-1|^2 \left(\frac{\upsilon}{\lambda}\right) \left[\frac{\Phi_b(ka)}{ka}\right] \tag{4}$$

where N_v, σ_b, and d denote the number of droplets per unit volume, the cross-sectional area of backward scattering, and the film thickness. And $m = n_{LC}/n_p$, which is the refractive index ratio of LC to polymer; a is the radius of LC droplets; λ is the wavelength of the incident light; and υ is volume fraction of LC droplets. N_v, σ_b, and Φ_b can then be expressed as,

$$N_v = \frac{3\upsilon}{4\pi a^3} \tag{5}$$

$$\sigma_b = \pi a^2 |m-1|^2 \Phi_b(ka) \tag{6}$$

$$\Phi_b(ka) = \frac{4}{9}(ka)^4 \int_{\frac{\pi}{2}}^{\pi} \left(1+\cos^2\theta_s\right) \times \left[\frac{3}{(k_s a)^3}\left(\sin k_s a - k_s a \cos k_s a\right)\right]^2 \times \left[1+\beta N_v \hat{h}(k_s, \upsilon, a)\right] \sin\theta_s \, d\theta_s \tag{7}$$

where k_s is related to the scattering angle θ_s between the propagation direction of the incident light and the scattered light where it can be described as $k_s = 2k \sin\frac{\theta_s}{2}$. The correlation factor β is 0 in the case of single scattering by a LC droplet, and 1 when correlation between scatterers is considered for multiple scattering events per droplet. The detailed correlation of scattering between droplets was discussed with $\hat{h}(k_s, \upsilon, a)$ [21]. When $\beta = 0$, backscattering will linearly increase while maintaining the droplet size associated with maximum backscattering as the volume fraction of LC droplets increases. When considering droplet correlation $\beta = 1$, the droplet size associated with maximum backscattering slightly shifts as the volume fraction increases. Assuming a non-absorbing and closed system, energy conservation necessitates $T = 1 - B$ where T represents the fractional light transmitted without scattering. Based on theoretical and experimental work, the fractional backscattering power B is maximized when the droplet radius a ranges from $\lambda/5$ to $\lambda/7$ while the volume fraction of droplets η ranges from 0.5 to 0.1 (Fig. S2) [20].

The scenarios of forward and backward scatterings or only forward scattering, which may represent analogies to Rayleigh and Mie scattering respectively, are illustrated in Fig. 1d. Even though blue light interacts with the color conversion layer and undergoes scattering, if

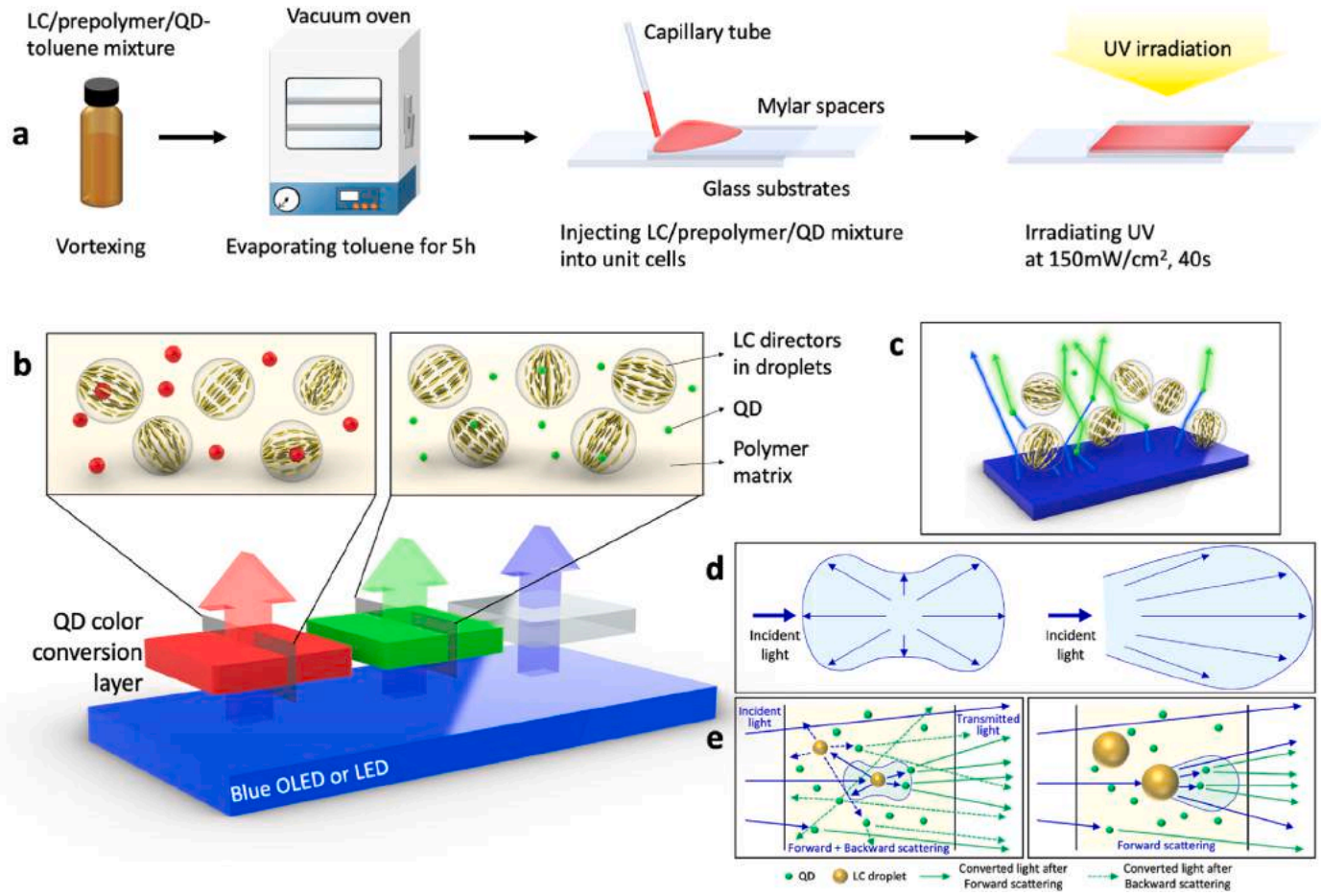

Fig. 1. Enhancement of color conversion efficiency in QD-OLEDs. **(a)** Schematic illustration of the fabrication process for a color conversion layer using quantum dot-liquid crystal-polymer (QD-LC-P) mixtures. **(b, c)** Schematic illustrations depicting the proposed LC scatterers with optical scattering within a color conversion layer. **(d)** Cases demonstrating occurrences of both backward and forward scatterings, or only forward scattering. **(e)** Schematic illustration showing how increased backward scattering lengthens the optical path within the composite layer, thereby increasing the probability that light interacts with QDs. (For interpretation of the references to color in this figure legend, the reader is referred to the Web version of this article.)

some portion of blue light is unconverted, unconverted blue light and converted light of each color emerge together and color mixed. We illustrate the schematic of light scattering caused by LC droplets in a polymer matrix when exposed to blue light in the color conversion layers in Fig. 1e. Note that this depiction exclusively focuses on the expression of converted light by QDs, disregarding absorbed or scattered light. In cases where the size of LC droplets is comparable to or larger than the wavelength of the incident light, the light predominately scatters forward. Conversely, when the droplets' size is smaller than the wavelength of the incident light, both backward and forward scattering occur, thereby extending the optical path. This extension increases the likelihood of interaction with QD particles, suggesting that a greater proportion of incident light can be effectively converted by QDs. We anticipate that achieving the maximum level of backward scattering will result in the highest light conversion efficiency.

2.2. The droplet size effect in scattering property of LC-P composite films

Building on theoretical foundations, we firstly carried out an analysis on PDLC unit cells of various droplet sizes, specifically those that do not contain QDs. The fabrication procedure for these was identical to that for QD color conversion films, with the sole difference being the absence of QDs in the mixtures. Factors such as UV irradiance and exposure time, LC concentration, and temperature significantly influence the size of LC droplets in PDLC films; these factors are detailed in Table 1. As shown by polarized optical microscopy (POM) images (upper-right insets of

Table 1
Sample condition of LC-P and QD-P composites with UV irradiance, exposure time.

Samples	S11[a]	S12	S13	S14	S15	S16	S17	S18	S19	S21R[b,c]	S22R	S23R	S24R
QD/[wt%]	–	–	–	–	–	–	–	–	–	10	20	30	40
E7/[wt%]	40	40	40	60	60	60	80	80	80	–	–	–	–
NOA65/[wt%]	60	60	60	40	40	40	20	20	20	90	80	70	60
TiO_2/[wt%]	–	–	–	–	–	–	–	–	–	–	–	–	–
UV irradiance/[mW/cm^2]	5	20	150	5	20	150	5	20	150	150	150	150	150
UV exposure time [sec]	1200	300	40	1200	300	40	1200	300	40	40	40	40	40

[a] S11-S19: LC-P.
[b] S21-S24: QD-P.
[c] R: red QD.

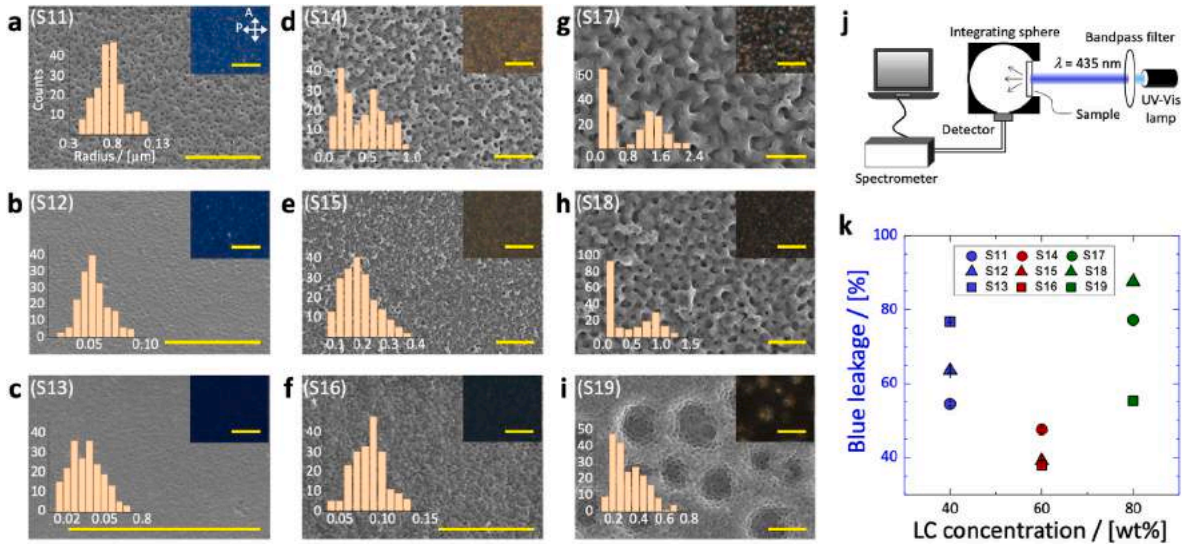

Fig. 2. Blue leakage ratio of LC-P composites based on changes in LC concentration. **(a–i)** Scanning electron microscopy (SEM) images of polymer matrices after the removal of LCs, reflecting changes in the composition of LC:P (E7:NOA65) and UV irradiance across samples S11-S19. The histograms in the lower-left insets indicate droplet size distribution as measured from SEM images, while polarizing optical microscopy (POM) images are displayed in the upper-right insets. Scare bars are 10 μm. **(j)** Schematic illustration of the optical setup for measuring external quantum efficiency (EQE) and blue light leakage ratio based on the wavelength of 435 nm. **(k)** Measurements of blue light leakage for LC-P composite samples S11-S19. (For interpretation of the references to color in this figure legend, the reader is referred to the Web version of this article.)

Fig. 2a–i), smaller LC droplets ($a < \sim 100$ nm) appear more bluish than larger ones ($a > \sim 100$ nm) within polymer matrices from which LCs have been removed due to scattering at this length scale. Scanning electron microscopy (SEM) images reveal variations in porosity within polymer morphology as depicted in Fig. 2a–i. The lower-left histograms within Fig. 2a–i and data provided in Table 2 offer information about droplet size distribution as measured from SEM images.

Based on the POM images taken from the real samples and theoretical framework on droplet size dependence on PIPS, we verified that an increase in LC concentration coupled with a decrease in irradiance of UV results in larger droplet size. This phenomenon can be attributed to a decrease in the polymerization rate and crosslinking density among prepolymer molecules when either the prepolymer concentration or UV intensity is reduced. In other words, as LC concentration increases, the droplet size increases because of the high fraction of LC. When UV intensity gets weak, the droplet size gets bigger because the polymerization rate is reduced [22,23]. Meanwhile, an intriguing observation was made with sample S19, which bore a resemblance to lunar craters. We interpret this as being due to high UV irradiance and high LC concentration triggering large-scale phase separation followed by smaller scale separation. Additionally, samples S14, S17, and S18 exhibited coexistence of large and small droplet size distributions. This implies a phase separation mechanism wherein smaller droplets aggregate to form larger ones [24].

The optical setup for measuring blue light leakage is illustrated in Fig. 2j. The forward-scattered transmitted blue light is integrated and quantified to evaluate blue light leakage ratio. As suggested by theoretical work, the fractional backward scattering power ($B = 1 - T$) increases as the volume fraction of LC droplets increases. Backward scattering can be maximized assuming that the radius a is approximately $\lambda/5$ and that the volume fraction of the system ranges from about 0.4 to 0.6 — similar to the range of LC concentrations used in our experiment. We note that when the correlation effect is high ($\beta \sim 1$), the droplet size contributing to maximum scattering shifts as the volume fraction increases. However, when $\beta \sim 0$, the droplet size contributing to maximum scattering remains almost consistent despite changes in volume fraction. In our experiment, sample S16 exhibited minimal blue light leakage as shown in Fig. 2k, with a droplet radius resembling $\lambda/5$–87 nm (at $\lambda =$ 435 nm). This result aligns well with expectations based on maximizing backward scattering under conditions involving UV irradiation at 150 mW/cm^2 for 40 s and weight fraction of the binary composite LC:P is approximately 60:40.

2.3. Optical properties and color conversion efficiency of QD-LC-P composite films

Transmission electron microscope (TEM) images and a schematic illustration of the synthesized red and green InP/ZnSe/ZnS QDs are presented in Fig. 3a–c and S3a. The TEM images reveal the lattice structure of the InP core, with the lattice fringes of red QD (RQD) and green QD (GQD) measuring 0.35 nm and 0.34 nm, respectively. In Fig. 3d and e, the measured absorption peaks of RQDs and GQDs were shown, respectively. The emission peaks for RQD and GQD were identified at 630 nm and 530 nm respectively, with their FWHM measured to be 41 nm for RQD, and 37 nm for GQD. QDs emit light at lower energy than they absorb; this energy difference, based on Stokes shift, is a phenomenon that occurs when electrons are transferred from the singlet excitation state to the singlet ground state, which represents recombination of the singlet excitons to emit light [25]. Fourier-transform infrared spectroscopy (FT-IR) was performed for verifying ligands attached to QDs (Fig. 3f,g, Fig. S3 and Experimental Section) such as oleic acid (OA), trioctylphosphine (TOP), and 1-dodecanethiol (DDT) as

Table 2
Measured average radius of LC droplets.

Sample	S11	S12	S13	S14	S15	S16	S17	S18	S19
Radii a/[nm]	75 ± 3	55 ± 3	40 ± 2	670 ± 140 275 ± 90	200 ± 65	90 ± 20	1450 ± 285 365 ± 90	875 ± 245 220 ± 45	4340 ± 880 440 ± 100 250 ± 55

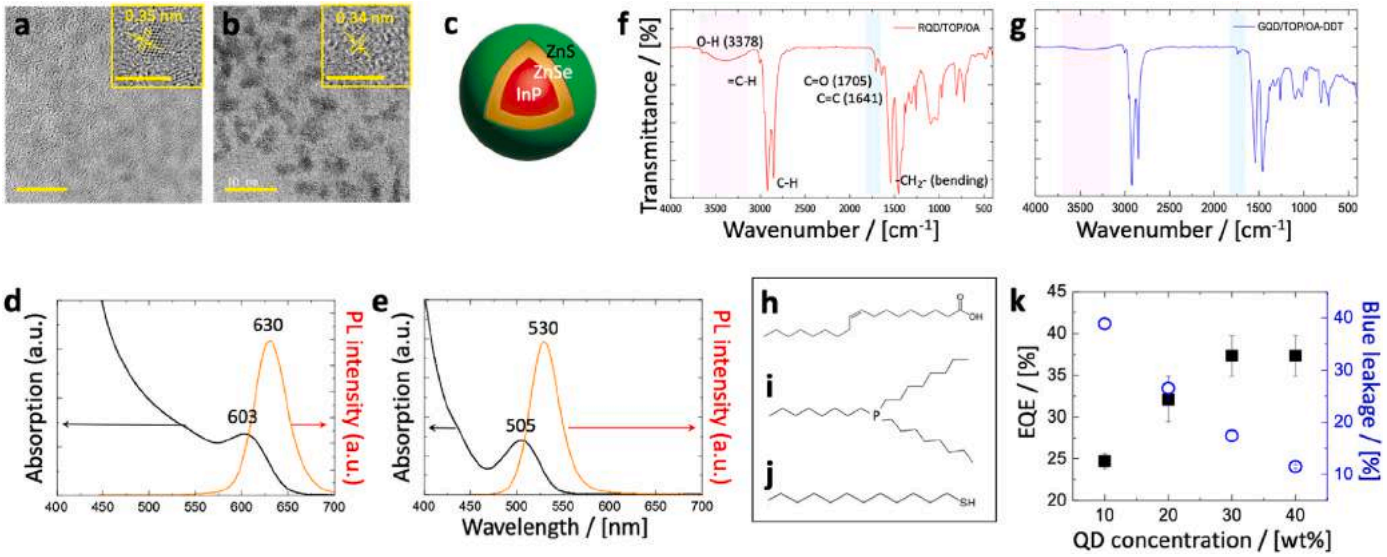

Fig. 3. Structures of QDs, EQE, and blue leakage ratio. **(a,b)** Transmission electron microscope (TEM) images of InP/ZnSe/ZnS: (a) RQD and (b) GQD. Scare bars are 10 nm and 5 nm in the insets. **(c)** Schematic illustration of the structure of InP/ZnSe/ZnS QDs. **(d,e)** Absorbance and photoluminescence (PL) for (d) RQD and (e) GQD. The excitation wavelength for PL is 435 nm. **(f,g)** Fourier-transform infrared spectroscopy (FT-IR) spectra for both (f) RQD and (g) GQD. **(h–j)** The molecular structures of (h) oleic acid (OA), (i) trioctylphosphine (TOP) and (j) 1-dodecanethiol (DDT). **(k)** Measurements of EQE of QD-P composite samples S21-S24 and blue light leakage based on the wavelength of 435 nm with changes in RQD concentration. (For interpretation of the references to color in this figure legend, the reader is referred to the Web version of this article.)

shown in Fig. 3h–j. In the case of DDT, S-H vibrational stretching mode at 2563 cm^{-1} was observed when measuring pure DDT disappears after treating GQD with DDT (Figs. S3b and c). In case of TOP, several literatures [26,27] reported the peaks for TOP at 1159, 1070, and 1023 cm^{-1}, suggesting C-P peaks of TOP as observed in the yellow region from 1000 to 1100 cm^{-1} in Fig. S3b for both RQD and GQD. We also measured EQE and blue leakage of QD-P composites (Table 1) across various QD concentrations as shown in Fig. 3k. The measurements indicate that EQE increases while blue leakage decreases as QD concentration increases. However, EQE appears to saturate around a concentration range of about 30~40 wt% in QD-P binary composites due to what is known as concentration quenching effect [6].

To verify the enhancement of EQE by LC scatterers, we prepared QD-LC-P composites with various LC concentrations as shown in Table 3. Photographs of the fabricated QD-LC-P in unit glass cells illuminated by a 455 nm blue light are shown in Fig. 4a. The numbers in Fig. 4a–c indicate the LC concentrations to the QD-LC-P composites. Changes in the brightness of the samples are noticeable with the naked eyes, and the strongest scattering occurs with the sample S35R or S35G (Table 3) when the weight fraction of QD:LC:P was 15:51:34 (if considering only LC:P, the fraction is 60:40). As the result shown in the previous section, the strongest backscattering occurs at this concentration due to the droplet size met with the Rayleigh-Gans approximation. In Fig. 4a, the photograph shows PL occurred from the samples under blue light. The brightness changes because of different scattering in the QD-LC-P layer. When backscattering is the strongest, more photons were detected by camera as also seen by eyes. We obtained POM images and PL optical microscopy images (inset) were obtained for both RQD (Fig. 4b) and GQD (Fig. 4c) with the optical setup for PL microscopy as schematically illustrated in Fig. 4d. The converted light is filtered through bandpass filters at 550 or 650 nm to block unwanted wavelengths. Clear PL images were obtained, with the brightest images observed. When the LC concentration is too low, dark states were observed in POM images due to the minimal scattering. As the LC concentration approaches the LC droplet size that produces the strongest backscattering for both RQD and GQD, brighter states begin to emerge. With further increases in LC concentration, larger LC droplets tend to be produced, which would induce more forward scattering than backward scattering.

EQE and blue leakage measurements were conducted on QD-LC-P composite samples containing RQD (Fig. 4e) and GQD (Fig. 4f), using a fixed QD concentration of approximately 15 wt%. In both RQDs and GQDs, EQE increased while blue leakage decreased as the LC concentration increased. Specifically, compared to each binary QD-P composite, EQE of when using an optimal LC concentration S35R or S35G (Table 3) is improved by 27.6% (EQE enhanced from 26.0% to 33.1%) for RQDs and 22.4% (EQE enhanced from 24.5% to 30.0%) for GQDs, which is consistent with observations made from POM and PL images in Fig. 4a and b,c. The backscattered light can increase the light path length

Table 3
Sample condition of QD-LC-P composites, cured under UV irradiance (150 mW/cm^2) and UV exposure time (40 s).

Samples	Ref.R[a,b] Ref.G[c]	S31R[d] S31G	S32R S32G	S33R S33G	S34R S34G	S35R S35G	S36R S36G	S37R S37G
QD/[wt%]	15.0	15.0	15.0	15.0	15.0	15.0	15.0	15.0
E7 (conc. to LC-P)[e]/[wt%]	–	17.0 (20)	25.5 (30)	34.0 (40)	42.5 (50)	51.0 (60)	59.5 (70)	68.0 (80)
NOA65 (conc. to LC-P)[e]/[wt%]	85.0 (100)	68.0 (80)	59.5 (70)	51.0 (60)	42.5 (50)	34.0 (40)	25.5 (30)	17.0 (20)
TiO_2/[wt%]	–	–	–	–	–	–	–	–

[a] Ref.: QD-P composites.
[b] R: red QD.
[c] G: green QD.
[d] S31-S37: QD-LC-P composites.
[e] Concentration when only considering LC-P.

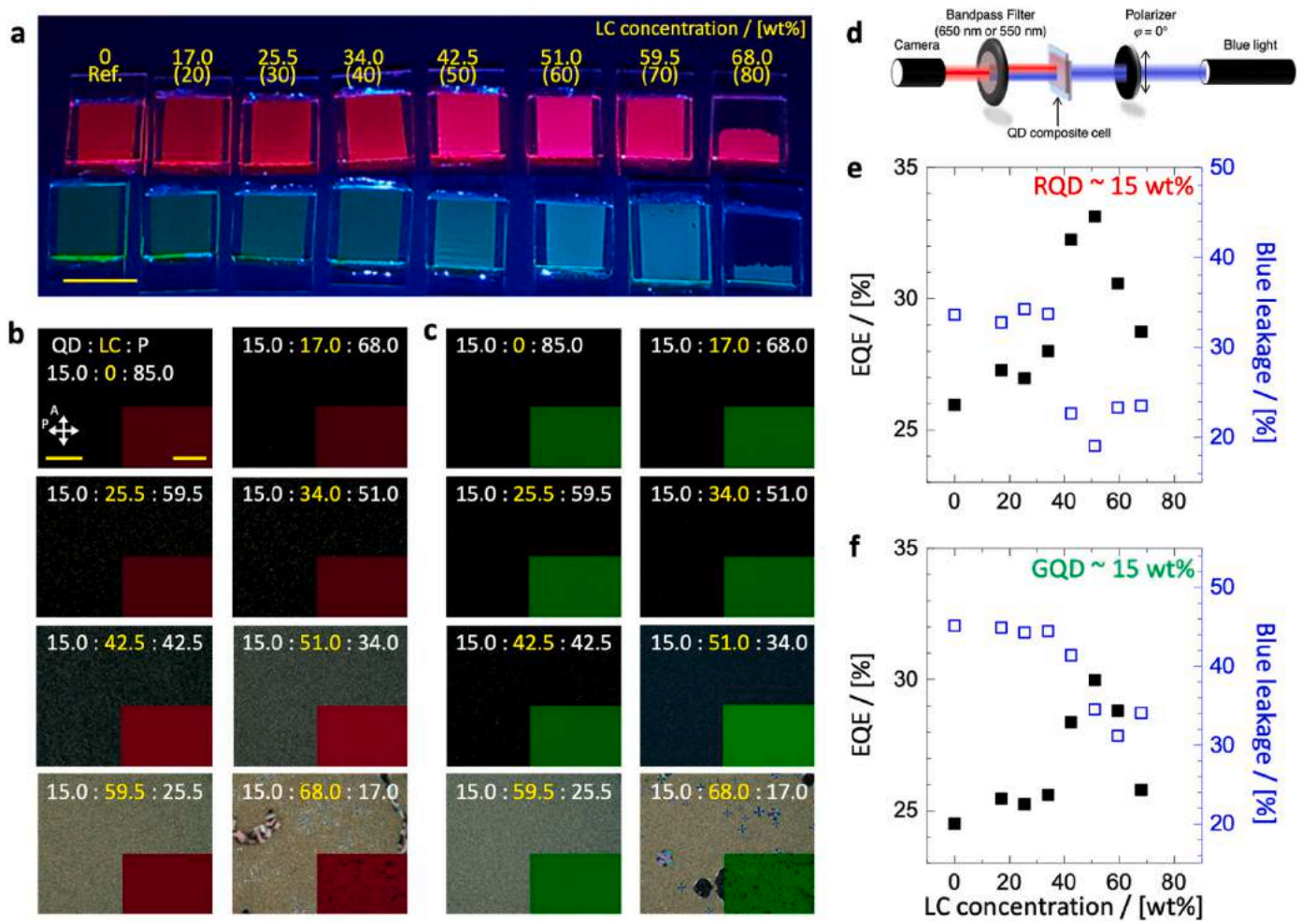

Fig. 4. Verification of color conversion properties of QDs. **(a)** Observed photoluminescence (PL) of QD-LC-P ternary composite samples under exposure to blue light at 455 nm. The numbers in the figures indicate LC concentration of the QD-LC-P composites and, in the parenthesis, LC concentration when considering only the weight fraction of LC:P. Scare bar is 4 cm. **(b,c)** POM images of (b) RQD and (c) GQD as the LC concentration varies. The insets show PL microscopy images of QD films, excited by light at 455 nm. Scare bars are 200 μm (500 μm in the insets). **(d)** Schematic illustration of the optical setup for PL optical microscopy. **(e,f)** EQE and blue leakage based on the wavelength of 435 nm for both (e) RQD and (f) GQD when LC concentrations change and the QD concentration is maintained at around 15%. (For interpretation of the references to color in this figure legend, the reader is referred to the Web version of this article.)

to enhance the color conversion efficiency of QDs by recycling the unconverted light within the composite layer.

2.4. Scattering properties when TiO_2 particles added to LC-P composite films

We mixed TiO_2 nanoparticles with NOA65 to verify its scattering properties. We tried various TiO_2 concentrations to verify the stability of mixtures for solution processes by injecting into empty cells, which would be similar to doing inkjet printing in practical manufacturing processes. After attaching OA to the TiO_2 nanoparticles (Fig. S4), we mixed OA-treated TiO_2 with toluene, and the OA-treated TiO_2 concentration was incrementally increased from 2 to 21 wt% as shown in Table 4. After fabrication of P-TiO_2 composites by UV cure, upon exposing samples to 455 nm blue light, brightness was observed to increase along with increasing TiO_2 concentration as shown in Fig. 5a. As the highest refractive index mismatch between polymer matrix and TiO_2 brings strong scattering, we used TiO_2 with the refractive index of 2.87 at 632.8 nm and average size of 210 nm. When the size of TiO_2 is approximately half of light wavelength, the optimum scattering can be achieved [28]. The bright field images of P-TiO_2 samples displayed in Fig. 5b show decreasing brightness with increasing concentrations of TiO_2 due to images being taken under the transmission mode of POM. In

Table 4
Sample condition of P-TiO_2 composites, cured under UV irradiance (150 mW/cm^2) and UV exposure time (40 s).

Samples	S41[a]	S42	S43	S44	S45	S46	S47
QD/[wt%]	–	–	–	–	–	–	–
E7 (conc. to LC-P)[b]/[wt %]	–	–	–	–	–	–	–
NOA65 (conc. to LC-P)[b]/[wt%]	98.0	96.0	94.0	92.0	88.0	84.0	79.0
TiO_2/[wt%]	2.0	4.0	6.0	8.0	12.0	16.0	21.0

[a] S41-S47: P-TiO2 composites.
[b] Concentration when only considering LC-P.

Fig. 5c, blue leakage measurements for P-TiO_2 composite samples were conducted. An increase in the concentration of TiO_2 led to an almost linear decrease in blue leakage because of their reflection in visible wavelength range including the 455 nm blue light.

EQE and blue leakage of QD-P-TiO_2 composite samples with various TiO_2 concentrations (Table 5) were measured as shown in Fig. 5d and e. Being agree with the result in Fig. 5c, blue leakage decreases linearly with increasing TiO_2 concentration. However, in terms of EQE, both red and green QD-P-TiO_2 composite samples exhibited saturation in the

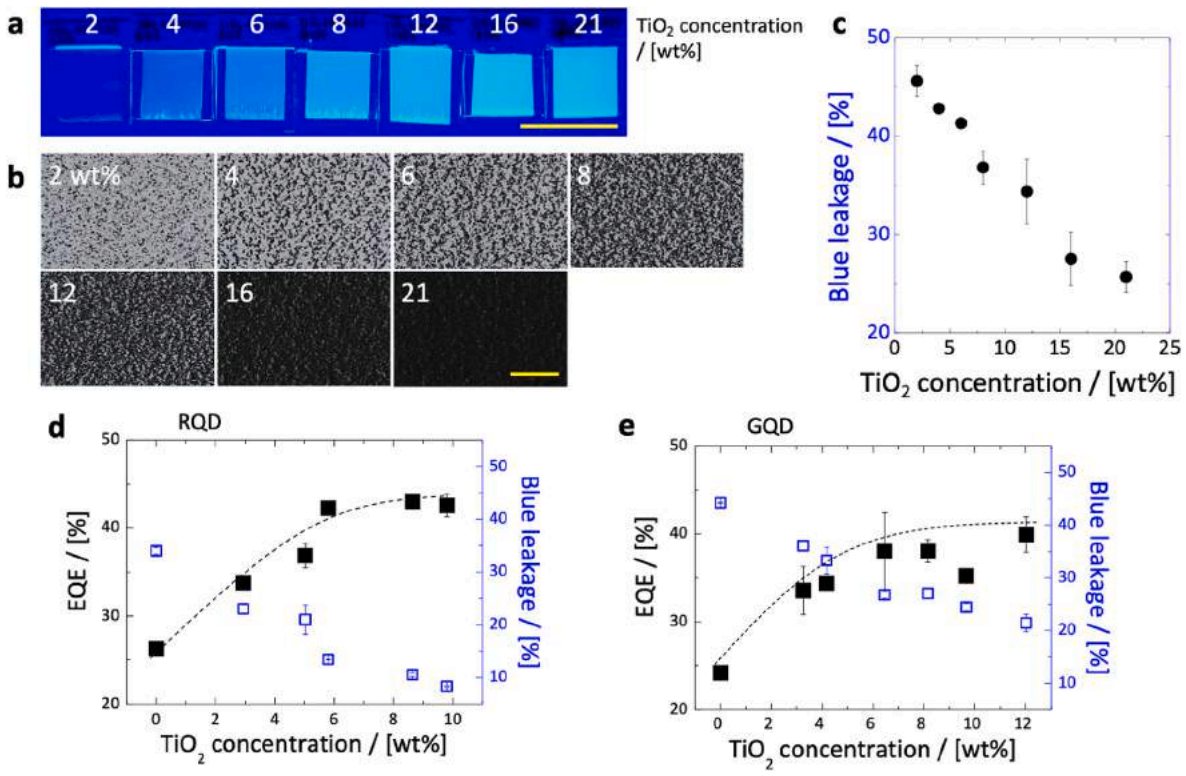

Fig. 5. Scattering properties of P-TiO_2 composite films and color conversion properties of QD-P-TiO_2 composite films. **(a)** Scattering observed in P-TiO_2 composite samples under exposure to blue light at 455 nm. The numbers in (a) represent the concentration of TiO_2. Scare bar is 4 cm. **(b)** POM images corresponding to each sample. Scare bar is 200 μm. **(c)** Blue leakage measurements of P-TiO_2 composites as a function of TiO_2 concentration based on the wavelength of 435 nm. **(d,e)** EQE and blue leakage measurements of QD-P-TiO_2 composite samples with (d) RQD and (e) GQD based on the wavelength of 435 nm. (For interpretation of the references to color in this figure legend, the reader is referred to the Web version of this article.)

Table 5
Sample condition of QD-P-TiO_2 composites, cured under UV irradiance (150 mW/cm^2) and UV exposure time (40 s).

Samples	S51R[a,b]	S52R	S53R	S54R	S55R	S56R	S51G[c]	S52G	S53G	S54G	S55G	S56G
QD/[wt%]	14.6	14.3	14.1	13.7	13.5	13.2	14.5	14.4	14.0	13.8	13.5	13.2
E7/[wt%]	–	–	–	–	–	–	–	–	–	–	–	–
NOA65/[wt%]	82.5	80.7	80.1	77.7	76.7	74.8	82.2	81.4	79.5	78.0	76.8	74.8
TiO_2/[wt%]	2.9	5.0	5.8	8.6	9.8	12.0	3.3	4.2	6.5	8.2	9.7	12.0

[a] S51-S56: QD-P-TiO2 composites.
[b] R: red QD.
[c] G: green QD.

values at the TiO_2 concentration of approximately 6 wt%. We discuss about this phenomenon with three possible reasons. First of all, small effect of the reduction in QD concentration as TiO_2 concentration increases in the mixtures might contribute to the EQE. Secondly, TiO_2 particles may couple with the QDs, which leads quenching. When the concentration of QD and TiO_2 reaches some point, charges may be transferred from QDs to TiO_2 particles due to the energy difference between their conduction bands although the ligands mostly insulate electron transferring [29,30]. Thirdly, based on the measured absorbance of TiO_2, the blue light absorption, which seemingly occur near 435 nm as shown in Fig. S5 [31], might slightly contribute to the EQE saturation.

Consequently, we selected a TiO_2 concentration less than 6 wt% for quaternary systems of QD-LC-P-TiO_2 composite samples to prevent the concentration quenching while keeping EQE as high as we can expect via additional LC scatterers as shown in Fig. 6. The sample conditions are outlined in Table 6. Fig. 6a shows photographs of QD-LC-P-TiO_2 composite samples with changes in the fraction of LC with TiO_2 concentration of approximately 6 wt%, which is observed under blue light at 455 nm. POM images in Fig. 6b and c reveal that phase separation occurs with different phase boundaries as LC concentration increases. Fig. 6d and e depict EQE and blue leakage for red and green QD-LC-P-TiO_2 quaternary composite samples as LC concentration varies. The EQE was improved by 75.3% (EQE enhanced from 26.5% to 46.4%) for the sample S63R (Table 6) when the weight fraction of QD:LC:P:TiO_2 was 14:31.8:47.7:6.5 (if considering only LC:P, the fraction is 40:60), and 81.9% (EQE enhanced from 23.6% to 42.9%) for the sample S63G (Table 6) when the weight fraction was 14.1:39.8:39.8:6.3 (if considering only LC:P, the fraction is 50:50), compared to each sample Ref.R (Table 6) and Ref.G (Table 6) binary composites as shown in Fig. 6d and e. In case of the QD-LC-P ternary composite samples, the maximum EQE was achieved with the samples S35R and S35G (Table 3) when the weight fraction of QD:LC:P was 15:51:34 (if considering only LC:P, the fraction is 60:40). If considering the fraction of only LC and P for these ternary and quaternary composites, the maximum EQE, i.e., the optimum LC scatterer size is achieved at different LC concentration with embedded TiO_2. We hypothesize that some fraction of UV light was absorbed by TiO_2 particles (as the spectrum shown in Fig. S5) during PIPS process, leading to larger LC scatterer sizes [32,33]. We attempted to find explanations by examining the morphology of the polymer

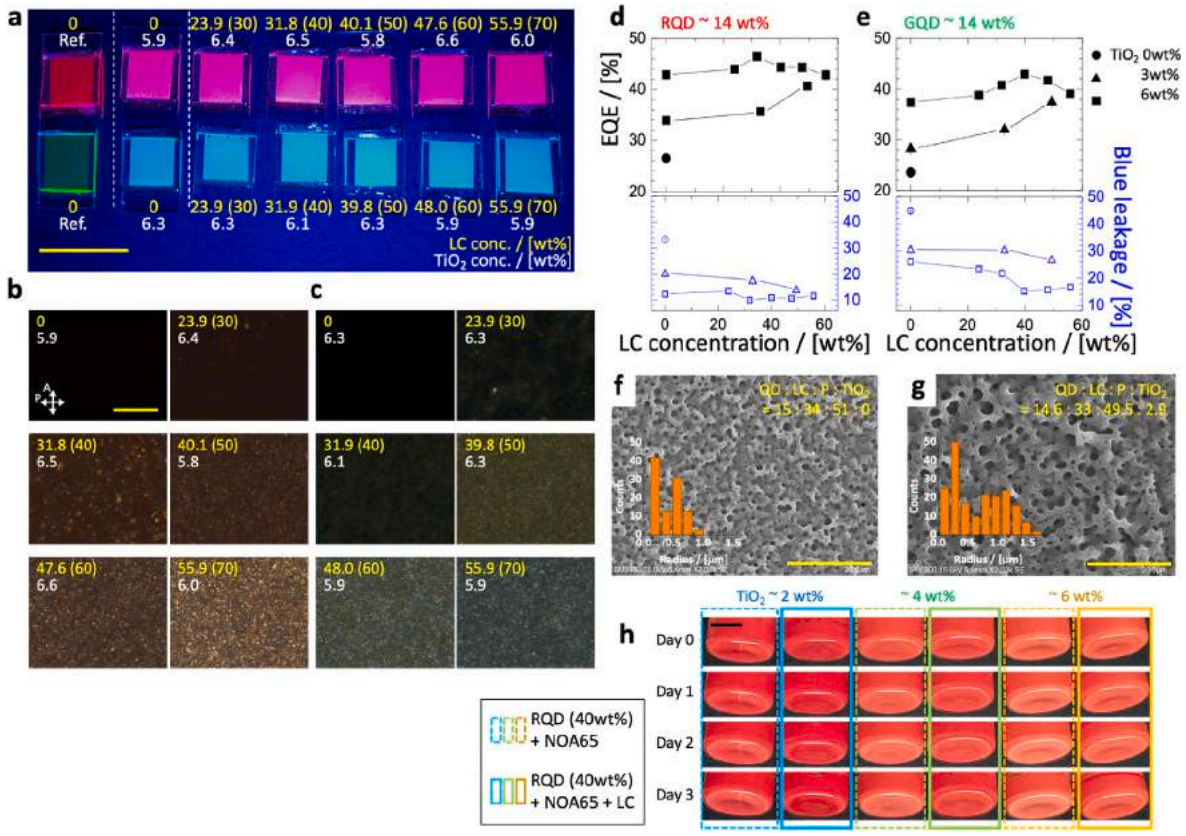

Fig. 6. Color conversion efficiency of QD-LC-P-TiO_2 composite samples. **(a)** PL images of samples exposed to blue light at 455 nm. Scale bar is 4 cm. **(b,c)** POM images of (b) red and (c) green QD-LC-P-TiO_2 composite samples, according to varying LC concentrations. The numbers in (a–c) with yellow fonts represent the LC concentration, while the numbers in parentheses indicate the LC concentration when only considering LC:P. The numbers with white fonts, TiO_2 concentration. Scare bar is 200 μm. **(d,e)** EQE and blue leakage measurements based on the wavelength of 435 nm for (d) red and (e) green QD-LC-P-TiO_2 composite samples as TiO_2 concentration changes from 0 to 6 wt% (It is a ternary system when TiO_2 is at 0 wt%). **(f,g)** Scanning electron microscopy (SEM) images along with inset histograms showing droplet size distribution for samples (f) without TiO_2 and (g) with approximately 3 wt% TiO_2. The ratio of LC:P (E7:NOA65) is maintained at 60:40 wt%. **(h)** Observations on sedimentation/aggregation of RQDs at a concentration of 40 wt% in both ternary (RQD-NOA65-TiO_2), and quaternary mixtures (RQD-E7-NOA65-TiO_2), with respect to varying concentrations of TiO_2 over a period of three days. Scale bar is 0.5 cm. (For interpretation of the references to color in this figure legend, the reader is referred to the Web version of this article.)

Table 6
Sample condition of QD-P-TiO_2 and QD-LC-P-TiO_2 composites, cured under UV irradiance (150 mW/cm^2) and UV exposure time (40 s).

Samples	Ref.R[a,b]	S61R[d]	S62R[e]	S63R	S64R	S65R	S66R	S67R[d]	S68R	S69R
QD/[wt%]	15.0	14.1	14.0	14.0	14.1	14.0	14.2	14.5	14.6	14.5
E7 (conc. to LC-P)[f]/[wt%]	–	–	23.9 (30)	31.8 (40)	40.1 (50)	47.6 (60)	55.9 (70)	–	33.0 (40)	49.4 (60)
NOA65 (conc. to LC-P)[f]/[wt%]	85.0 (100)	80 (100)	55.7 (70)	47.7 (60)	40.1 (50)	31.8 (40)	23.9 (30)	82.5 (100)	49.5 (60)	32.9 (40)
TiO_2/[wt%]	–	5.9	6.4	6.5	5.8	6.6	6.0	3.0	2.9	3.2
Samples	Ref.G[a,c]	S61G[d]	S62G[e]	S63G	S64G	S65G	S66G	S67G[d]	S68G	S69G
QD/[wt%]	15.0	14.1	14.1	14.2	14.1	14.1	14.2	14.5	14.5	14.5
E7 (conc. to LC-P)[d]/[wt%]	–	–	23.9 (30)	31.9 (40)	39.8 (50)	48.0 (60)	55.9 (70)	–	32.8 (40)	49.4 (60)
NOA65 (conc. to LC-P)[d]/[wt%]	85.0 (100)	79.6 (60)	55.7 (70)	47.8 (60)	39.8 (50)	32.0 (40)	24.0 (30)	82.2 (100)	49.2 (60)	32.9 (40)
TiO_2/[wt%]	–	6.3	6.3	6.1	6.3	5.9	5.9	3.3	3.5	3.2

[a] Ref.: QD-P composites from Table S3.
[b] R: red QD.
[c] G: green QD.
[d] S61, S67: QD-P-TiO_2 composites.
[e] S62-S66 and S68-S69: QD-LC-P-TiO_2 composites.
[f] Concentration when only considering LC-P.

matrix of the sample S16 (Table 1) LC-P binary composite and another LC-P-TiO_2 ternary composite as SEM images are shown in Fig. 6f and g. While maintaining the weight fraction LC:P at 60:40, S16 contained no TiO_2 whereas the other LC-P-TiO_2 had TiO_2 of about 3 wt%. SEM images revealed larger pore sizes when TiO_2 was added (Fig. 6g), compared to when it was absent (Fig. 6f). With lower UV irradiance, the optimum LC scatterer size is made at relatively lower LC concentration because the higher the UV intensity and the lower the LC concentration, smaller LC droplets are produced. It is also important to note that the amounts of TiO_2 slightly vary across the samples, making it difficult to attribute maximum EQE solely to the strongest scattering of blue light at a specific size of LC droplets. However, this discrepancy might be negligible

because, for example, in the case of RQD, EQE of S63R is higher with TiO_2 concentration (6.5 wt%), compared to another sample S65R, containing the highest TiO_2 concentration (6.6 wt%).

To further explore the issue of aggregation or sedimentation of inorganic particles, which can cause significant problems in solution processes such as solution degradation or clogging of inkjet nozzles, we examined the mixture solutions of RQD-P-TiO2 and RQD-LC-P-TiO_2 as depicted in Fig. 6h. Adding LC to QD-P-TiO_2 mixtures enhances the dispersion of TiO_2 particles and improves the aggregation issue (Fig. S6). However, as TiO_2 concentration increases to reach ~6 wt%, the TiO_2 particles aggregate at the bottom of vials. At a concentration of ~4 wt%, the initially observed one seems promising but after three days, aggregation/sedimentation occurs. For a concentration of ~2 wt%, almost no aggregation occurs (columns within dotted rectangles in Fig. 6h). Conversely, when mixed with LCs, aggregation issues improved significantly as shown in the columns within solid rectangles in Fig. 6h and S6.

Furthermore, high concentrations of TiO_2 may cause excessive reflection of external light as observed in Fig. 6a. We checked that a TiO_2 concentration around 3 wt% would be almost perfectly stable for most solution processes and would exhibit less reflection. We also confirmed that NOA65 provides good miscibility for quaternary mixtures by experimenting with different types of prepolymers within these mixtures (Fig. S7). Finally, we measured EQE and blue leakage for QD-LC-P-TiO_2 composite samples with approximately 3 wt% TiO_2; these measurements are represented by solid and empty triangle markers on Fig. 6d and e. The EQE was improved by 53.4% (EQE enhanced from 26.5% to 40.6%) for red and 58.6% (EQE enhanced from 23.6% to 37.4%) for green QD-LC-P-TiO_2 composite samples compared to their respective QD-P binary composite samples.

3. Conclusion

QDs are promising materials for next-generation displays due to their narrow FWHM, high PLQY, and suitability for solution-based processes. We fabricated QD color conversion films using potential combinations of either ternary QD-LC-P or quaternary QD-LC-P-TiO_2 composites. These composites can generate scatterers, either LC droplets via PIPS method or a combination of LC droplets and TiO_2 inorganic nanoparticles. The results revealed that LC scatterers produced by the PIPS method with a LC:P ratio of 60:40 can optimally reduce blue leakage due to effective LC scatterer sizes (~87 nm). This significant reduction corresponds to approximately $\lambda/7$ where λ ~435 nm. By incorporating these LC scatterers, we achieved notable increases in EQE for ternary QD-LC-P films. When the weight fraction of LC:P (E7:NOA65) is 60:40, the EQE increments reached approximately 27.6% (EQE enhanced from 26.0% to 33.1%) for RQDs and about 22.4% (EQE enhanced from 24.5% to 30.0%) for GQDs compared to QD-P binary composite films. Moreover, we successfully developed quaternary QD-LC-P-TiO_2 composites which enhanced EQE up to 81.9% (EQE enhanced from 23.6% to 42.9% for GQD, when the weight fraction of LC:P is 50:50 with TiO_2 of 6 wt%) and 58.6% (EQE enhanced from 23.6% to 37.4% for GQD when the weight fraction of LC:P is 40:60 with TiO_2 of 3 wt%). This work offers an efficient approach towards realizing high color-purity displays with minimal usage of inorganic nano-scatterers—ensuring no aggregation occurs during inkjet printing processes without nozzle clogging or solution degradation through sedimentation. Our findings not only open avenues for surpassing existing performance standards set by current QD-OLEDs but also contribute valuable insights into scattering mechanisms for EQE enhancement.

4. Experimental Section

4.1. Materials

We fabricated a QD-LC-P composite scatterer using a liquid crystal (LC) mixture (E7, $T_{NI} = 59–60$ °C, $n = 1.5962$, $n_e = 1.7464$, $n_o = 1.5211$, $\Delta n = 0.2253$ at 589 nm, Merck Advanced Technologies Co., Ltd.), which comprises of 51% n-pentylcyanobiphenyl, 25% n-heptylcyanobiphenyl,16% n-octyloxycyanobiphenyl and 8% n-pentylcyanoterphenyl. We also used prepolymer (NOA65, $n = 1.524$, maximum optical absorption at 350–380 nm by Norland Products Inc.) composed of trimethylpropane diallyl ether, trimethylopropane tristhiol and isophorone diisocyanate ester with benzophenone photo-initiator. The synthesized QDs (Daeyeon Chemicals Co., Ltd.) dispersed in toluene, which consist of InP/ZnSe/ZnS with emission peaks at both 630 nm and 530 nm using ligands trioctylphosphine (TOP)/oleic acid (OA) and TOP/OA-1-dodecanethiol (DDT), respectively, were further characterized. FT-IR measurement for RQD (Fig. 3f) and GQD (Fig. 3g) showed strong peaks at 3378 cm^{-1} (-O-H), 1705 cm^{-1} (C=O), and 1641 cm^{-1} (C=C). At 2854 cm^{-1}, 2915 cm^{-1}, 801 cm^{-1}, and 715 cm^{-1}, C-H stretching modes for CH_2 and CH_3 groups were observed. The bending vibration of CH_2 is assigned at 1467 cm^{-1}. However, given that all three ligands include the hydrocarbon chain, distinguishing them by using these peaks is challenging. In the case of DDT, the presence of thiol groups shows the peak related to the S-H vibrational stretch mode at 2563 cm^{-1} as depicted in the FT-IR spectrum of pure DDT. This peak disappears for GQD after treating GQD with DDT (Fig. S3c). Strong peaks in the yellow region (Fig. S3a) between 1000 and 1100 cm^{-1} were observed in both RQD and GQD. Several literatures suggest C-P stretching peaks of TOP at 1159, 1070, and 1023 cm^{-1} [26,27]. As shown in the FT-IR spectra of pure ligands (Fig. S3a), TOP has noticeable peaks in that yellow region. Although the possibility of phosphate existence from the synthesis residue still cannot be ignored [34], we are able to determine the TOP attached on both RQD and GQD as other reports also suggests these peaks caused by InP capped with TOP [35,36]. We used nanoparticles as another scatterer (TiO_2, $n = 2.87$ at 632.8 nm, rutile type, average size = 210 nm, Sinopro Co., LTD.) *n*-hexane (Samchun Chemical Co., LTD.) with ligand, OA (technical grade, 90%, Sigma Aldrich) to homogenously disperse in toluene. In addition to NOA65, various prepolymers were compared for their miscibility with QDs and TiO_2. These included UV curable resin (acrylate based prepolymer, low viscosity, Sigma Aldrich), NOA61 (thiol-ene based prepolymer, Norland Products, Inc), NOA74 (acrylate based prepolymer, Norland Products, Inc), NOA1348 (fluorinated prepolymer, Norland Products, Inc). It is well-known that organic acids like OA can enhance the dispersibility of TiO_2 nanoparticles in non-polar organic solvents [33]. This is due to the OH group on the surface of TiO_2 reacting with OA's carboxylic group while its long aliphatic chain tail enables stable dispersion within the organic solvent [32]. Thus we treated TiO_2 with OA for even dispersion within our QD/prepolymer mixture. To do this we added 100 mL of *n*-hexane and 1g of OA into a beaker, mixed uniformly using a magnetic stirrer set at 60 °C, 200 rpm for 10 min. After that, 1 g of TiO_2 powder was added, mixed at 60 °C, 200 rpm for 4 h, filtered using a vacuum filter, and washed 3 to 4 times with deionized (DI) water and isopropyl alcohol (IPA) to remove residual materials. The obtained wet powder was dried in a vacuum oven at 100 °C for 24 h before use. To test dispersion stability, small amounts of OA-treated TiO_2 and untreated TiO_2 were added to the toluene solvent. After vortexing, the degree of precipitation over time was observed. As shown in Fig. S4, untreated TiO_2 particles immediately clumped and precipitated while OA-treated TiO_2 particles remained uniformly dispersed within the toluene.

4.2. Cell fabrication process

To fabricate the color conversion layer, QDs dispersed in toluene were uniformly mixed with the LC/prepolymer mixture using a vortex mixer. The toluene was then removed in a vacuum oven over 5 h. The composition of the LC/prepolymer varies depending on specific conditions, and the ratio of QDs is maintained at 15 wt% relative to the LC/prepolymer mixture for both RQD and GQD. TiO_2 was added in a weight ratio to the total mixture and homogeneously mixed with a magnetic stirrer at 200 rpm for 2 h. The final mixture was injected into a unit cell

using capillary action. This cell consisted of two glass substrates sandwiched with a 10 μm Mylar spacer, and it was then cured under specified conditions using an LED UV light source (HH200-sp4, U-Hitec Co., LTD.) with a peak wavelength of 365 nm. UV intensity was measured using a UV irradiance meter (UIT-201, Ushio). Unless otherwise specified, UV irradiation was conducted at 150 mW/cm^2 for 40 s. All preparation processes for the mixture and cell fabrication were conducted at room temperature to minimize damage to the QDs. The rationale behind fabricating the color conversion layer in unit-cell form through injection is two folds: it maintains constant thickness and simulates ink jetting from a nozzle. The average cell thickness is 12 ± 0.52 μm.

4.3. Characterization

To measure cell thickness, we employed the concept of a Fabry-Perot interferometer using a UV–Vis light source (DH-2000-BAL, Ocean Insight), optical fiber (QR600-7-SR-125F, Ocean Insight), and spectrometer (USB2000+, Ocean Insight). A polarized optical microscope (POM, Eclipse LV100 N POL, Nikon) was used to analyze the samples' optical properties. Photographs were captured with a CCD camera (DS-Ri2, Nikon). For QD characterization, lattice structure images were taken with a Cs-corrected field emission transmission electron microscope (STEM, JEM-ARN200F, JEOL). We utilized a FT-IR (Frontier, Perkin Elmer) employing the attenuated total reflection method to analyze ligand compositions of RQD and GQD. Absorbance spectrum observations were made through a UV–Vis spectrometer (V-730, JASCO Inc.), and photoluminescence properties were analyzed using spectrofluorophotometer (RF-6000, Shimadzu Europe). Additionally, to observe surface morphology where phase separation between LCs and polymers occurred, *n*-hexane and dichloromethane were mixed in a 7:3 ratio. The unit cells were then immersed for a day before drying. This process dissolves the LC from the polymer matrix. For observation using variable pressure scanning electron microscopy (SEM, SU3900 Hitachi), the obtained polymer films were coated with platinum for 150 s by RF sputtering to provide conductivity and prevent charge accumulation. Post-image processing was performed using open-source software (ImageJ, NIH) to calculate average sizes of cavities along with standard deviation. We randomly measured 200 cavities per sample. Finally, to measure blue light scattering properties of films containing scatterers we used both UV–Vis spectrum analysis and an integrating sphere.

4.4. External quantum efficiency and blue leakage ratio

To evaluate the blue light scattering, light extraction ability, and color purity of the fabricated film, we defined and measured the EQE and blue leakage. We designed an optical setup using an integrating sphere (2P4/M, Thorlabs), optical fiber (QP600-1-SR-BX, Ocean Insight), and the spectrometer. A blue light with a peak wavelength of 435 nm was irradiated onto the sample by attaching a band-pass filter to a UV–Vis light source (LC8, Hamamatsu).

4.5. Fluorescent images

An optical set-up was designed to take a fluorescent image of QD film excited by blue light. A blue LED (3W Royal Blue, Mightex Systems.) with a wavelength of 455 nm was connected to the POM, and the light intensity was controlled by an LED controller (SLC-MA series, Mightex Systems.). The blue light is linearly polarized and passed through the QD film. To observe the emitted light, the leaked blue light was blocked with a bandpass filter (Edmund optics) with a center wavelength of 650 or 550 nm and a FWHM of 50 nm. Other settings were kept constant during image capture.

We designed an optical setup to capture a fluorescent image of the QD film excited by blue light. A blue LED (3W Royal Blue, Mightex Systems) with a wavelength of 455 nm was connected to the POM, and its light intensity was controlled using an LED controller (SLC-MA series, Mightex Systems). The blue light, once linearly polarized, passed through the QD film. To observe the emitted light, we blocked leaked blue light using a band-pass filter (Edmund Optics) with a center wavelength of either 650 or 550 nm and a FWHM of 50 nm. All other settings were maintained constant during image capture.

Funding

The Ministry of Education (National Research Foundation) grant 2021R1I1A1A01060001 (MSK).

The Ministry of Science and ICT (National Research Foundation) grant 2022R1A2C2091671 (SHL).

Competing financial interests

The authors declare no competing financial interests.

CRediT authorship contribution statement

MinSu Kim: Writing – review & editing, Writing – original draft, Visualization, Supervision, Funding acquisition, Conceptualization. **DaYeon Lee:** Writing – original draft, Visualization, Methodology, Investigation. **HaYoung Jung:** Visualization, Investigation. **Seung Hee Lee:** Writing – review & editing, Supervision, Funding acquisition, Conceptualization.

Declaration of competing interest

We declare that we have no known competing financial interests or personal relationships that could have appeared to influence the work reported in this paper.

Data availability

Data will be made available on request.

Acknowledgements

This work was supported by Basic Science Research Program through the National Research Foundation (NRF) of Korea, funded by the Ministry of Education, Korea [2021R1I1A1A01060001]; by the Ministry of Science and ICT (MSIT), Korea [2022R1A2C2091671]; and by the Commercialization Promotion Agency for R&D Outcomes (COMPA) grant, funded by the Ministry of Science and ICT, Korea [RS-2023-00304743].

Appendix A. Supplementary data

Supplementary data to this article can be found online at https://doi.org/10.1016/j.compositesb.2024.111425.

References

[1] Jung J, Park HB, Jung HY, Jung SE, Kim SG, Kim TH, et al. Recent progress in liquid crystal devices and materials of TFT-LCDs. J Inf Dis 2023;25:121–42. https://doi.org/10.1080/15980316.2023.2281224.

[2] Jang E, Jun S, Jang H, Lim J, Kim B, Kim Y. White-light-emitting diodes with quantum dot color converters for display backlights. Adv Mater 2010;22:3076–80. https://doi.org/10.1002/ADMA.201000525.

[3] Chen J, Hardev V, Hartlove J, Hofler J, Lee E. 66.1: distinguised paper: a high-efficiency wide-color-gamut solid-state backlight system for LCDs using quantum dot enhancement film. SID Symp Dig Tech Pap 2012;43:895–6. https://doi.org/10.1002/J.2168-0159.2012.TB05931.X.

[4] Ekimov AI, Efros AL, Onushchenko AA. Quantum size effect in semiconductor microcrystals. Solid State Commun 1985;56:921–4. https://doi.org/10.1016/S0038-1098(85)80025-9.

[5] Shirasaki Y, Supran GJ, Bawendi MG, Bulović V. Emergence of colloidal quantum-dot light-emitting technologies. Nat Photonics 2013;7:13–23. https://doi.org/10.1038/nphoton.2012.328.

[6] Tilley RJD. Colour and the optical properties of materials: an exploration of the relationship between light, the optical properties of materials and colour. John Wiley and Sons; 2010. https://doi.org/10.1002/9780470974773.
[7] Li JS, Tang Y, Li ZT, Li Z, Ding XR, Rao LS. Investigation of the emission spectral properties of carbon dots in packaged LEDs using TiO2 nanoparticles. IEEE J Sel Top Quant Electron 2017;23:2000507. https://doi.org/10.1109/JSTQE.2017.2729023.
[8] Li F, Jiang J, Zhang Q, Wei J, Song Y, Li Q, et al. Enhancing extraction efficiency of quantum dot light-emitting diodes by surface engineering. Opt Express 2017;25:17683–94. https://doi.org/10.1364/OE.25.017683.
[9] Tang Y, Li Z, Li ZT, Li JS, Yu SD, Rao LS. Enhancement of luminous efficiency and uniformity of CCT for quantum dot-converted LEDs by incorporating with ZnO nanoparticles. IEEE Trans Electron Dev 2018;65:158–64. https://doi.org/10.1109/TED.2017.2771785.
[10] Xie B, Liu H, Hu R, Wang C, Hao J, Wang K, et al. Targeting cooling for quantum dots in white QDs-LEDs by hexagonal boron nitride platelets with electrostatic bonding. Adv Funct Mater 2018;28:1801407. https://doi.org/10.1002/ADFM.201801407.
[11] Wang S, Dou X, Chen L, Fang Y, Wang A, Shen H, et al. Enhanced light out-coupling efficiency of quantum dot light emitting diodes by nanoimprint lithography. Nanoscale 2018;10:11651–6. https://doi.org/10.1039/C8NR02082E.
[12] Li ZT, Li JX, Li JS, Deng ZH, Deng YH, Tang Y. Scattering effect on optical performance of quantum dot white light-emitting diodes incorporating SiO nanoparticles. IEEE J Quant Electron 2020;56:3600109. https://doi.org/10.1109/JQE.2020.2986018.
[13] Hyun BR, Sher CW, Chang YW, Lin Y, Liu Z, Kuo HC. Dual role of quantum dots as color conversion layer and suppression of input light for full-color micro-LED displays. J Phys Chem Lett 2021;12:6946–54. https://doi.org/10.1021/acs.jpclett.1c00321.
[14] Li J, Tang Y, Li Z, Ding X, Yu B, Lin L. Largely enhancing luminous efficacy, color-conversion efficiency, and stability for quantum-dot white LEDs using the two-dimensional hexagonal pore structure of SBA-15 mesoporous particles. ACS Appl Mater Interfaces 2019;11:18808–16. https://doi.org/10.1021/acsami.8b22298.
[15] Montgomery GP. Angle-dependent scattering of polarized light by polymer-dispersed liquid-crystal films. J Opt Soc Am B 1988;5:774–84. https://doi.org/10.1364/JOSAB.5.000774.
[16] Park NH, Noh SC, Nayek P, Lee M-H, Kim MS, Chien L-C, et al. Optically isotropic liquid crystal mixtures and their application to high-performance liquid crystal devices. Liq Cryst 2015;42:530–6. https://doi.org/10.1080/02678292.2015.1006698.
[17] Lim YJ, Kang M, Jeon HS, Kim MS, Lee SH. Low-temperature processable transparent liquid crystal light shutter. J Mol Liq 2022;368. https://doi.org/10.1016/j.molliq.2022.120823.
[18] Lee SL, Kim MS, Lee DY, Lin YH, Lee SH. Optically isotropic nano-size encapsulation of nematic liquid crystals with a high-filling factor. J Mol Liq 2022;359:119254. https://doi.org/10.1016/J.MOLLIQ.2022.119254.
[19] Pagidi S, Kim MS, Manda R, Ahn S, Jeon MY, Hee Lee S. Ideal micro-lenticular lens based on phase modulation of optically isotropic liquid crystal-polymer composite with three terminals. J Mol Liq 2023;380. https://doi.org/10.1016/j.molliq.2023.121730.
[20] M Jr GP, Vaz NA, Smith GW. Effect of accelerators on the structure, solar attenuation characteristics and electro-optic performance of polymer-dispersed liquid crystal films. Mol Cryst Liq Cryst Sci Technol Sect A 1993;225:131–51. https://doi.org/10.1080/10587259308036224.
[21] Montgomery GP, Vaz NA. Light-scattering analysis of the temperature-dependent transmittance of a polymer-dispersed liquid-crystal film in its isotropic phase. Phys Rev 1989;40:6580. https://doi.org/10.1103/PhysRevA.40.6580.
[22] Drzaic PS. Liquid crystal dispersions. Singapore: World Scientific Publishing Co. Pte. Ltd.; 1995.
[23] Lucchetti L, Gobbi L, Simoni F. Analysis of the phase separation process in UV cured polymer dispersed liquid crystals for optical applications. Mol Cryst Liq Cryst Sci Technol Sect A 2001;359:89–96. https://doi.org/10.1080/10587250108035570.
[24] Lovinger AJ, Amundson KR, Davis DD. Morphological investigation of UV-curable polymer-dispersed liquid-crystal (PDLC) materials. Chem Mater 1994;6:1726–36. https://doi.org/10.1021/cm00046a027.
[25] Nirmal M, Norris DJ, Kuno M, Bawendi MG, Efros AL, Rosen M. Observation of the “dark exciton” in CdSe quantum dots. Phys Rev Lett 1995;75:3728. https://doi.org/10.1103/PhysRevLett.75.3728.
[26] Lu X, Korgel BA, Johnston KP. High yield of germanium nanocrystals synthesized from germanium diiodide in solution. Chem Mater 2005;17:6479–85. https://doi.org/10.1021/cm0515956.
[27] Chen S, Zhang X, Zhang Q, Tan W. Trioctylphosphine as both solvent and stabilizer to synthesize CdS nanorods. Nanoscale Res Lett 2009;4:1159–65. https://doi.org/10.1007/s11671-009-9375-x.
[28] Ohenoja K, Illikainen M, Niinimäki J. Effect of operational parameters and stress energies on the particle size distribution of TiO2 pigment in stirred media milling. Powder Technol 2013;234:91–6. https://doi.org/10.1016/J.POWTEC.2012.09.038.
[29] Hyun BR, Zhong YW, Bartnik AC, Sun L, Abruña HD, Wise FW, et al. Electron injection from colloidal PbS quantum dots into titanium dioxide nanoparticles. ACS Nano 2008;2:2206–12. https://doi.org/10.1021/nn800336b.
[30] Chakrapani V, Tvrdy K, Kamat PV. Modulation of electron injection in CdSe-TiO2 system through medium alkalinity. J Am Chem Soc 2010;132:1228–9. https://doi.org/10.1021/ja909663r.
[31] Rajabathar JR, Al-Lohedan HA, Arokiyaraj S, Issa ZA, Dash CS, Murugesan S, et al. Characterization of pure rutile titania nanoparticle prepared by feasible method for coatings and visible light-driven dye removal application. Coatings 2021;11:1150. https://doi.org/10.3390/COATINGS11101150.
[32] Wu X, Wang D, Yang S. Preparation and characterization of stearate-capped titanium dioxide nanoparticles. J Colloid Interface Sci 2000;222:37–40. https://doi.org/10.1006/JCIS.1999.6582.
[33] Jalili MM, Davoudi K, Zafarmand Sedigh E, Farrokhpay S. Surface treatment of TiO2 nanoparticles to improve dispersion in non-polar solvents. Adv Powder Technol 2016;27:2168–74. https://doi.org/10.1016/J.APT.2016.07.030.
[34] Paschalis EP, DiCarlo E, Betts F, Sherman P, Mendelsohn R, Boskey AL. FTIR microspectroscopic analysis of human osteonal bone. Calcif Tissue Int 1996;59:480–7. https://doi.org/10.1007/BF00369214/METRICS.
[35] Khanna PK, Jun KW, Hong KB, Baeg JO, Mehrotra GK. Synthesis of indium phosphide nanoparticles via catalytic cleavage of phosphorus carbon bond in n-trioctylphosphine by indium. Mater Chem Phys 2005;92:54–8. https://doi.org/10.1016/J.MATCHEMPHYS.2004.12.029.
[36] Lasheen D, Fathy M, Othman HA, Elkholy MM, Kashyout AEHB. Synthesis and characterization of InP quantum dots for photovoltaics applications. J Mater Sci Mater Electron 2023;34:1–12. https://doi.org/10.1007/S10854-023-10179-2.